





Control of Spin Polarization through Recollisions

Stefanos Carlström ^{1,2,*}, Jan Marcus Dahlström ², Misha Yu Ivanov ^{1,3,4}, Olga Smirnova ^{1,5} and Serguei Patchkovskii¹

¹Max-Born-Institut, Max-Born-Straße 2A, 12489 Berlin, Germany

²Department of Physics, Lund University, Box 118, SE-221 00 Lund, Sweden

³Department of Physics, Imperial College London, South Kensington Campus, SW72AZ London, United Kingdom

⁴Institut für Physik, Humboldt-Universität zu Berlin, Newtonstraße 15, 12487 Berlin, Germany

⁵Technische Universität Berlin, Ernst-Ruska-Gebäude, Hardenbergstraße 36A, 10623 Berlin, Germany

(Dated: October 9, 2023)

Using only linearly polarized light, we study the possibility of generating spin-polarized photoelectrons from xenon atoms. No net spin polarization is possible, since the xenon ground state is spin-less, but when the photoelectron are measured in coincidence with the residual ion, spin polarization emerges. Furthermore, we show that ultrafast dynamics of the recolliding photoelectrons contribute to an apparent flipping of the spin of the photoelectron, a process that has been completely neglected so far in all analyses of recollision-based processes. We link this phenomenon to the “spin–orbit clock” of the remaining ion. These effects arise already in dipole approximation.

Published in: *Physical Review A* **108**(4), 043104 (2023), DOI: [10.1103/PhysRevA.108.043104](https://doi.org/10.1103/PhysRevA.108.043104)

Keywords: Spin polarization, ultrafast spin–orbit interaction, above-threshold ionization, rescattering

I. INTRODUCTION

Generation of spin-polarized photoelectrons using intense circularly polarized light has recently become a topic of great interest [1–5]. Since the rare gases commonly employed in strong-field ionization experiments are spin-less in the ground state, linearly polarized light cannot generate net spin polarization. In this article we show that when the photoelectron is measured in coincidence with the final ion state, the spin polarization approaches 100 % in the individual ionization channels (resolved on J and M_J). Furthermore, we link the resulting spin polarization to the rescattering electron imaging the ultrafast hole motion, providing an intuitive picture of electron trajectories that contribute to an apparent spin flip of the detected electron — a signature of recollision-driven coupling between continua with different spins. We find that the spin-flip recollisions are very significant, and that we may exercise precise control over the outcome. This effect, which has so far been overlooked, is important in all recollision-based imaging techniques such as laser-induced electron diffraction [6], electron holography [7], and orbital tomography [8, 9].

This article is arranged as follows: section II introduces the computational tools we employ in the calculations, presented in section III. Section IV concludes the article.

II. THEORY

Our method consistently treats multi-electron spin dynamics in strong laser fields, and is thus suitable for our chosen target, xenon. It is based upon the time-dependent configuration-interaction singles (TD-CIS) [10–12]. The equations of motion (EOMs) describe the time evolution of the amplitude c_0 for the Hartree–Fock (HF) reference state, and the particle orbital

$|\tilde{k}\rangle$ emanating from the initially occupied (time-independent) orbital $|k\rangle$. Below, we employ Hartree atomic units. Quantities appearing on one side only are summed/integrated over. The different particle–hole channels can couple via both the laser interaction and the Coulomb interaction:

$$\begin{aligned} i\partial_t c_0 &= \langle k | \hat{V}_L | \tilde{k} \rangle, \\ i\partial_t |\tilde{k}\rangle &= (-\epsilon_k + \hat{f}) |\tilde{k}\rangle + c_0 \hat{V}_L |k\rangle - \langle l | \hat{V}_L | k \rangle |\tilde{l}\rangle \\ &\quad - (\hat{J}_{lk} - \hat{K}_{lk}) |\tilde{l}\rangle - \lambda_{\tilde{k}m} |m\rangle, \end{aligned} \quad (1)$$

where ϵ_k is the eigenvalue of the initially occupied orbital $|k\rangle$. The Fock operator is defined as $\hat{f} \stackrel{\text{def}}{=} \hat{h} + \hat{J}_{mm} - \hat{K}_{mm}$, with the one-body Hamiltonian containing the interaction with the external laser field, $\hat{h} \stackrel{\text{def}}{=} p^2/2 + \hat{V}_C(\mathbf{r}) + \hat{V}_L$, $\hat{V}_L \stackrel{\text{def}}{=} \mathbf{F}(t) \cdot \mathbf{r}$, and \hat{J}_{cd} and \hat{K}_{cd} are the *direct* and *exchange interaction* potentials, respectively (see Appendix A 1). The Lagrange multipliers $\lambda_{\tilde{k}m}$ in Equation (1) ensure that $|\tilde{k}\rangle$ at all times remains orthogonal to all initially occupied orbitals $|m\rangle$.

To implement spin–orbit coupling, instead of resorting to the full four-component Dirac–Fock treatment (RTDCIS [13]), we rely on the phenomenological two-component treatment of Peterson *et al.* [14]. It includes corrections due to scalar-relativistic effects, and at the same time reduces the number of electrons we need to treat explicitly. It replaces the scalar potential \hat{V}_C by the relativistic effective core potential (RECP), which models the atomic nucleus and the 1s–3d electrons of xenon according to

$$\hat{V}^{\text{RECP}}(\mathbf{r}) = \hat{V}^{\text{scalar}}(\mathbf{r}) + \mu \hat{V}_{\ell j}^{\text{s-o}}(\mathbf{r}). \quad (2)$$

The RECP allows us to identify effects associated with spin–orbit dynamics by scaling the spin–orbit splitting as

$$\Delta E_{\text{s-o}}(\mu) \approx \mu \Delta E_{\text{s-o}}(1), \quad (3)$$

where $\Delta E_{\text{s-o}}(1) \approx 1.4$ eV is the nominal spin–orbit splitting of the ionic ground state at the CIS level; the dependence is essentially linear in μ (see Appendix A 2).

* stefanos@mbi-berlin.de; stefanos.carlstrom@matfys.lth.se

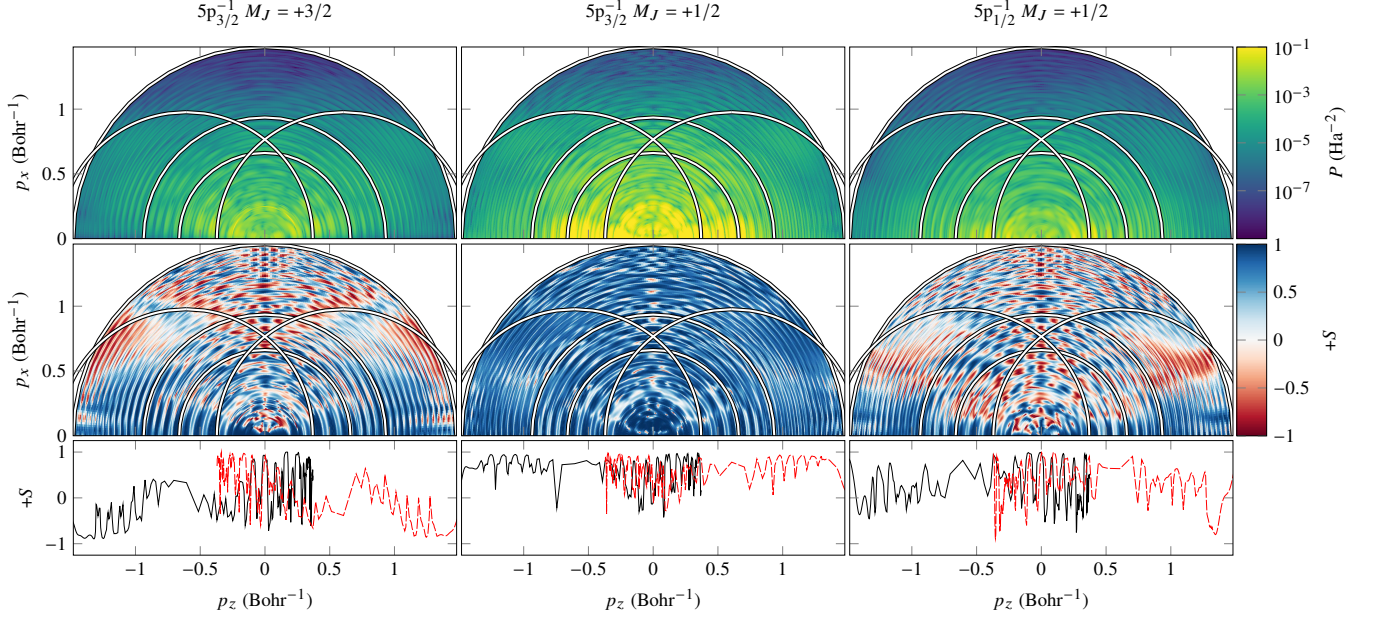


FIG. 1. *Top row*: Angularly resolved ATI spectra from xenon, correlated to different ionic channels. *Middle row*: Spin polarization of the photoelectrons; for $M_J < 0$, the spin polarization is exactly the opposite of the positive case. Blue colour means excess of spin-up (spin-down) for $+S$ ($-S$), and vice versa for red. The overlaid concentric circles indicate momenta at the detector corresponding to kinetic energies $2U_p$, $4U_p$, $10U_p$, respectively. The offset circles mark the contribution of recolliding electrons with the maximum possible return energy $W_{k,\max}$. *Bottom row*: Lineouts along the $W_{k,\max}$ circles in the middle row; the black solid (red dashed) line corresponds to initial ionization towards positive (negative) p_z .

The spin polarization is given by

$$S_I(E, \theta) \stackrel{\text{def}}{=} \frac{P_{I\alpha}(E, \theta) - P_{I\beta}(E, \theta)}{P_{I\alpha}(E, \theta) + P_{I\beta}(E, \theta)},$$

where $P_{I\sigma_z}(E, \theta)$ is the ion-, kinetic energy-, angle-, and spin-resolved photoelectron distribution (see Appendix A 3).

III. CALCULATIONS

We study above-threshold ionization (ATI) from xenon, with the following ionization channels included: $5p_{3/2}^{-1}$, $M_J = \pm 3/2, \pm 1/2$, and $5p_{1/2}^{-1}$, $M_J = \pm 1/2$ [15]. Ionization from 5s and lower-lying orbitals is strongly suppressed in the laser fields we consider [$\hbar\omega = \Delta E_{s-o}(1)$ and $I_0 = 44 \text{ TW/cm}^2$]. The *spin-mixed* channels $5p_{3/2}^{-1}$, $M_J = \pm 1/2$ (formed from linear combinations of $p_0\alpha$, $p_+\beta$ and $p_0\beta$, $p_-\alpha$, respectively) are preferentially ionized, since ionization in linearly polarized fields is dominated by p_0 [16].

The weaker channels $5p_{3/2}^{-1}$, $M_J = \pm 3/2$ are expected to be *spin-pure*, since to form the orbitals $5p_{3/2}$, $m_j = \pm 3/2$, the orbital- and spin-angular momenta must be maximally aligned ($p_+\alpha$ and $p_-\beta$, respectively). Linearly polarized electric fields preserve spin, and thus we expect that the outgoing electron is spin-pure as well. However, the results of our numerical simulations are surprising: only direct, on-axis photoelectrons maintain their expected spin (see Figure 1). In contrast electrons that have undergone recollision with the parent ion, and

are able to travel off-axis, exhibit substantial amounts of the opposite spin.

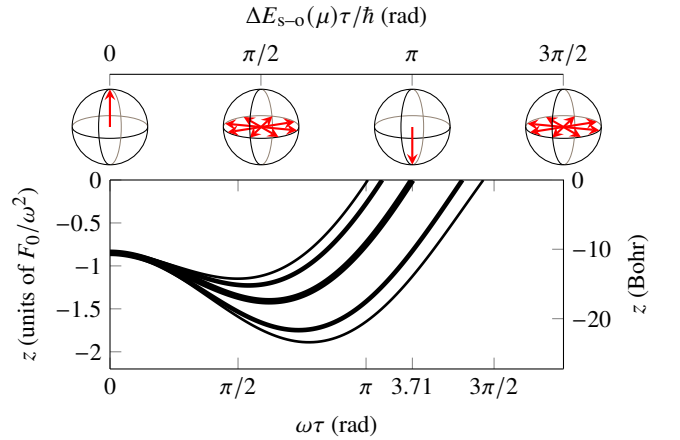


FIG. 2. Sketch of the proposed spin-flipping mechanism; the electron moves along a rescattering trajectory with an excursion phase of $\omega\tau$, which in the example is chosen such that the trajectory with maximum return energy $W_{k,\max}$, shown as the heaviest line, matches half a revolution of the spin-orbit clock, illustrated as Bloch spheres. The classical trajectories start at the tunnel exit of a Coulombic barrier.

To explain this behaviour, we posit that this effect results from the recollision of the returning electron off of the ion, which in the spin-mixed channels has time-evolving spin [1, 5]. Directly after ionization, the ion has a spin opposite that of

the photoelectron, yielding vanishing spin overall. If upon return, the electron finds an ion with a spin different from that at time of ionization, inelastic scattering into the spin-pure channels $5p_{3/2}^{-1}$, $M_J = \pm 3/2$ may contribute to photoelectrons of opposite spin in these channels. Furthermore, this apparent spin flip will predominantly occur when $\Delta E_{s-o}\tau \approx \pi$, where τ is the excursion time of the electron, see Figure 2 and the SI (see Appendix B). This dynamic corresponds to the *spin-orbit clock* in the ion undergoing half a revolution.

To investigate this hypothesis in a minimally invasive manner, we tune the spin-orbit splitting ΔE_{s-o} by changing the value of μ in (2), while keeping all remaining parameters constant. We then find

$$\pi \approx \Delta E_{s-o}(\mu)\tau = \frac{\Delta E_{s-o}(\mu)}{\omega}\omega\tau = \frac{\Delta E_{s-o}(\mu)}{\Delta E_{s-o}(1)}\omega\tau, \quad (4)$$

since we chose the photon energy to be in resonance with the nominal spin-orbit splitting, $\omega = \Delta E_{s-o}(1)$. Using (3), we get

$$\mu \approx \frac{\Delta E_{s-o}(\mu)}{\Delta E_{s-o}(1)} \approx \frac{\pi}{\omega\tau}. \quad (5)$$

For electrons returning with maximal kinetic energy, $W_{k,\max}$, which return at $\omega\tau \approx 3.71$, we obtain $\mu \approx 0.85$. It is easy to find those final momenta (combinations of p_z and p_x) which result from trajectories recolliding with $W_{k,\max}$ [17] (see Appendix B); these are marked in Figure 1 with circles in the forward ($p_z > 0$) and backward ($p_z < 0$) directions. If we take lineouts of the spin polarization along these circles, we predominantly measure the contribution of trajectories returning with $W_{k,\max}$ kinetic energy. The red streaks in Figure 1 that indicate the opposite spin do not fall perfectly on the $W_{k,\max}$ circle; this is mostly due to the circle being derived for classical trajectories with no potential present. The slight shift in momentum for the apparent spin flips is a result of Coulomb focusing.

We thus expect large amounts of opposite spin in the high-rescattering region ($|W_k| > 4U_p$), for $\mu \approx 0.85$, since the *spin-orbit clock* has undergone half a revolution, by the time electron returns. In Figure 3 we see that this is indeed the case, in the spin-pure channels $5p_{3/2}^{-1}$, $M_J = \pm 3/2$. Generalizing this argument, for $\mu \approx \frac{n\pi}{\omega\tau} = 0.85, 1.69, 2.54, 3.40, 4.23, 5.07, \dots$ we expect to see enhancement and suppression of the opposite spin for odd n and even n , respectively.

It is also interesting to note that for $\mu = 0$, the photoelectrons in the spin-pure channel are spin-pure as well. In this case, the period of the *spin-orbit clock* is $\frac{2\pi}{\Delta E_{s-o}(0^+)} = +\infty$, and the hole remains forever in its initial spin state, preventing any opposite spin appearing in the spin-pure channels.

To further explore the proposed mechanism, we selectively remove the Coulomb repulsion interaction from the EOMs (1); first we exclude exchange-type interactions between ionization channels by dropping the \hat{K}_{lk} term, and then the direct-type interchannel interactions \hat{J}_{lk} . Dropping the self-interaction correction \hat{K}_{mm} does not influence the spin polarization appreciably (see Appendix C 1). The intrachannel interactions \hat{J}_{mm} must remain, since otherwise the problem would reduce to a hydrogenic one with a bare xenon nucleus. We compare

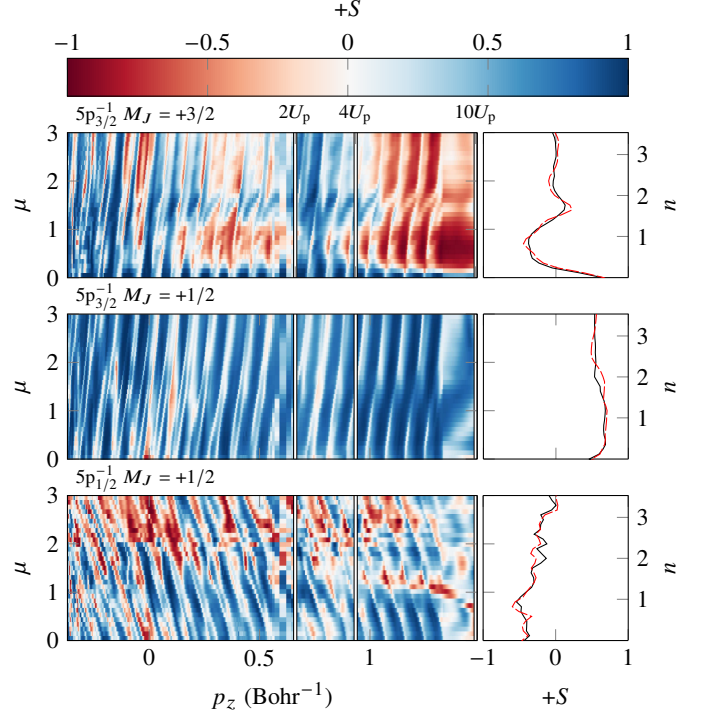


FIG. 3. Lineouts along the $W_{k,\max}$ circles in Figure 1, for a range of values of the spin-orbit scaling parameter μ [see Equation (3)], plotted as a function of p_z ; note that $2W_k = p_z^2 + p_x^2$, and the lineouts are *not* taken along constant p_x . As in Figure 1, for $M_J < 0$, the spin polarization is exactly $-S$. Each row corresponds to a specific ion channel; *top row* the spin-pure channel $5p_{3/2}^{-1}$, $M_J = +3/2$, *middle row* $5p_{3/2}^{-1}$, $M_J = +1/2$, *bottom row* $5p_{1/2}^{-1}$, $M_J = +1/2$. The *left column* shows emission in the forward direction, i.e. positive final p_z [due to the long pulse duration, $\tau = 15$ fs, the spin polarization is almost symmetric about $p_z = 0$ (see Appendix B 1)]. The *right column* shows the integrated spin polarization along the lineout, from $p^2/2 = 4U_p$ to p_{\max} ; the solid, black line corresponds to the forward emission, and the dashed red to the backward emission. The right ordinate indicate the expected positions corresponding to $n \approx \mu\omega\tau/\pi$ half-revolutions of the spin-orbit clock, for $\omega\tau \approx 3.71$ (see main text).

these instrumented calculations with the full Hamiltonian in Figure 4. As we see in the figure, the largest effect is the removal of \hat{J}_{lk} , which is the only term of the three which is long-range (\hat{K} , being traceless, decays at least as quickly as r^{-2}). We also note that the removal of \hat{K}_{lk} quantitatively changes the angular distribution of the spin polarization, even enhancing it, which suggests that \hat{K}_{lk} actually works *counter* to the proposed mechanism.

We now understand the mechanism leading to the opposite spin in the spin-pure channel better: The hole in this channel is also spin-pure, and as such does not undergo any spin oscillation in the *spin-orbit clock*. However, the holes in the other channels are spin-mixed, and the *spin-orbit clock* oscillates with the period $T_{s-o} \stackrel{\text{def}}{=} \frac{2\pi}{\Delta E_{s-o}(\mu)}$. After rescattering at the right moment, we may observe opposite spins due to inelastic scattering into $5p_{3/2}^{-1}$, $M_J = \pm 3/2$. Removing \hat{J}_{lk} from the

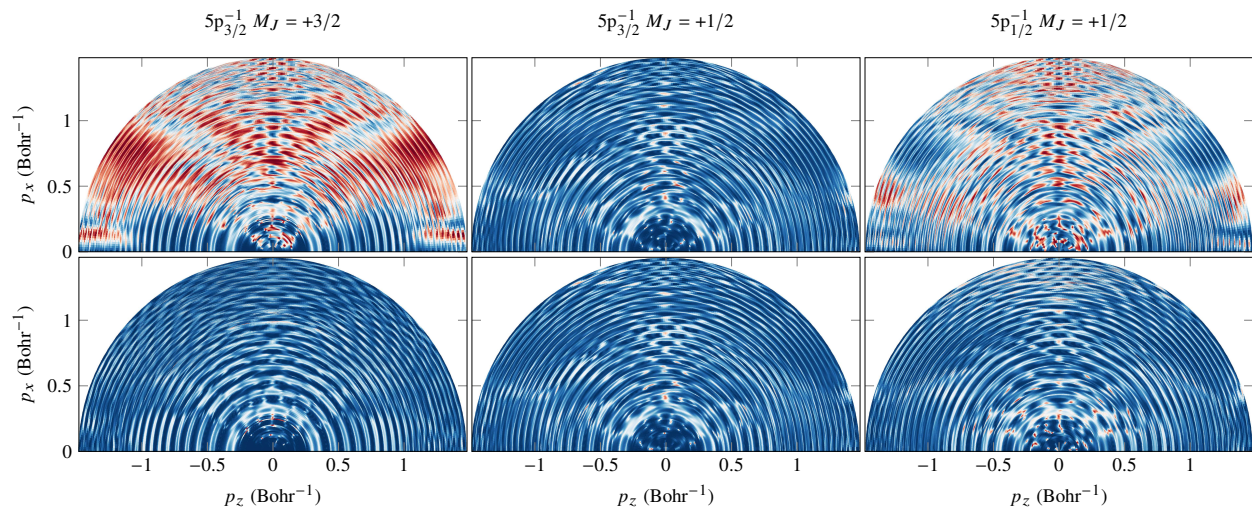


FIG. 4. Effect on the spin polarization when gradually removing the Coulomb electron–electron repulsion interaction from the EOMs (1). *Top row*: \hat{K}_{lk} dropped; *bottom row*: $\hat{K}_{lk}, \hat{J}_{lk}$ dropped. See the second row of Figure 1 for the case where all terms in the Hamiltonian are included.

EOMs (1) suppresses inelastic scattering, and thus precludes any transfer of spin between channels, as we see in Figure 4. This mechanism can be semi-quantitatively investigated by considering the explicit time–spin dependence of \hat{J}_{lk} and \hat{K}_{lk} in LS coupling, where the orbitals l and k change their spin with the period T_{s-o} (see Appendix C 2).

IV. CONCLUSIONS

In conclusion, we have demonstrated that we can generate spin-polarized electrons, even when ionizing using linearly polarized light, as long as we detect the photoelectrons in coincidence with the ion. Furthermore, due to the recollision mechanism in strong-field ionization, we are also able to control the spin of the photoelectron, by tuning the ratio of the spin–orbit splitting and the angular frequency of the driving field. This mechanism has important implications for recollision-based

imaging techniques such as laser-induced electron diffraction, which use the energy– and angle-resolved distribution of the photoelectron to infer the state of the ion; through the spin–orbit interaction, the spin of the photoelectron would reveal additional information on the entangled photoion.

ACKNOWLEDGMENTS

SCM would like to thank Edvin Olofsson for illuminating discussions. The work of SCM has been supported through scholarship 185-608 from *Olle Engkvists Stiftelse*. JMD acknowledges support from the *Knut and Alice Wallenberg Foundation* (2017.0104 and 2019.0154), the Swedish Research Council (2018-03845) and *Olle Engkvists Stiftelse* (194-0734). MI acknowledges support from *Horizon 2020 research and innovation* (899794). OS acknowledges support from *Horizon Europe* ERC-2021-ADG (101054696 *Uliisses*).

-
- [1] I. Barth and O. Smirnova, *Journal of Physics B: Atomic, Molecular and Optical Physics* **47**, 204020 (2014).
 - [2] A. Hartung, F. Morales, M. Kunitski, K. Henrichs, A. Laucke, M. Richter, T. Jahnke, A. Kalinin, M. Schöffler, L. P. H. Schmidt, M. Ivanov, O. Smirnova, and R. Dörner, *Nature Photonics* **10**, 526 (2016).
 - [3] D. Trabert, A. Hartung, S. Eckart, F. Trinter, A. Kalinin, M. Schöffler, L. P. H. Schmidt, T. Jahnke, M. Kunitski, and R. Dörner, *Physical Review Letters* **120**, 043202 (2018).
 - [4] Z. Nie, F. Li, F. Morales, S. Patchkovskii, O. Smirnova, W. An, N. Nambu, D. Matteo, K. A. Marsh, F. Tsung, W. B. Mori, and C. Joshi, *Physical Review Letters* **126**, 054801 (2021).
 - [5] N. Mayer, S. Beaulieu, Á. Jiménez-Galán, S. Patchkovskii, O. Kornilov, D. Descamps, S. Petit, O. Smirnova, Y. Mairesse, and M. Y. Ivanov, *Physical Review Letters* **129**, 173202 (2022).
 - [6] T. Zuo, A. Bandrauk, and P. Corkum, *Chemical Physics Letters* **259**, 313 (1996).
 - [7] Y. Huismans, A. Rouzee, A. Gijbetsen, J. H. Jungmann, A. S. Smolkowska, P. S. W. M. Logman, F. Lepine, C. Cauchy, S. Zamith, T. Marchenko, J. M. Bakker, G. Berden, B. Redlich, A. F. G. van der Meer, H. G. Muller, W. Vermin, K. J. Schafer, M. Spanner, M. Y. Ivanov, O. Smirnova, D. Bauer, S. V. Popruzhenko, and M. J. J. Vrakking, *Science* **331**, 61 (2010).
 - [8] S. Patchkovskii, Z. Zhao, T. Brabec, and D. M. Villeneuve, *Physical Review Letters* **97**, 123003 (2006).
 - [9] S. Patchkovskii, Z. Zhao, T. Brabec, and D. M. Villeneuve, *The Journal of Chemical Physics* **126**, 114306 (2007).
 - [10] N. Rohringer, A. Gordon, and R. Santra, *Physical Review A* **74**, 043420 (2006).
 - [11] L. Greenman, P. J. Ho, S. Pabst, E. Kamarchik, D. A. Mazziotti, and R. Santra, *Physical Review A* **82**, 023406 (2010).

- [12] S. Carlström, M. Spanner, and S. Patchkovskii, *Physical Review A* **106**, 043104 (2022), editors' Suggestion; S. Carlström, M. Bertolino, J. M. Dahlström, and S. Patchkovskii, *Physical Review A* **106**, 042806 (2022).
- [13] F. Zapata, J. Vinbladh, A. Ljungdahl, E. Lindroth, and J. M. Dahlström, *Physical Review A* **105**, 012802 (2022).
- [14] K. A. Peterson, D. Figgen, E. Goll, H. Stoll, and M. Dolg, *The Journal of Chemical Physics* **119**, 11113 (2003).
- [15] The quantum numbers J and M_J pertain to the states of the ion, whereas j and m_j label the initially occupied orbitals; for CIS from closed valence shells, $J = j$ and $M_J = -m_j$. In LS coupling, the p spin-orbitals are labelled $p_{m_\ell \sigma_z}$, where the possible values for m_ℓ are 0, \pm , and $\sigma_z = \alpha, \beta$ corresponding to spin-up/down.
- [16] A. Perelomov, V. Popov, and M. Terent'ev, *Soviet Physics Journal of Experimental and Theoretical Physics* **23**, 924 (1966).
- [17] M. Spanner, O. Smirnova, P. B. Corkum, and M. Y. Ivanov, *Journal of Physics B: Atomic, Molecular and Optical Physics* **37**, L243 (2004).
- [18] M. Dolg and X. Cao, *Chemical Reviews* **112**, 403 (2011).
- [19] M. Dolg, Relativistic effective core potentials, in *Handbook of Relativistic Quantum Chemistry*, Handbook of Relativistic Quantum Chemistry (Springer Berlin Heidelberg, 2016) pp. 449–478.
- [20] E. B. Saloman, *Journal of Physical and Chemical Reference Data* **33**, 765 (2004).
- [21] J. E. Hansen and W. Persson, *Phys. Scr.* **36**, 602 (1987).
- [22] W. Fritsch and C.-D. Lin, *Physics Reports* **202**, 1 (1991).
- [23] A. M. Ermolaev, I. V. Puzynin, A. V. Selin, and S. I. Vinitzky, *Physical Review A* **60**, 4831 (1999).
- [24] A. M. Ermolaev and A. V. Selin, *Physical Review A* **62**, 015401 (2000).
- [25] V. V. Serov, V. L. Derbov, B. B. Joulakian, and S. I. Vinitzky, *Physical Review A* **63**, 062711 (2001).
- [26] L. Tao and A. Scrinzi, *New Journal of Physics* **14**, 013021 (2012).
- [27] A. Scrinzi, *New Journal of Physics* **14**, 085008 (2012).
- [28] F. Morales, T. Bredtmann, and S. Patchkovskii, *Journal of Physics B: Atomic, Molecular and Optical Physics* **49**, 245001 (2016).
- [29] P. B. Corkum, *Physical Review Letters* **71**, 1994 (1993).
- [30] D. A. Varshalovich, *Quantum Theory of Angular Momentum: Irreducible Tensors, Spherical Harmonics, Vector Coupling Coefficients, 3nj Symbols* (World Scientific Pub, Singapore Teaneck, NJ, USA, 1988).

Appendix A: Methods

1. Coulomb Repulsion

The *direct* and *exchange interaction* potentials are defined by their action on a spin-orbital

$$\begin{aligned} \hat{J}_{cd} |e\rangle &\stackrel{\text{def}}{=} \chi_e(\varsigma_1) \int \frac{d\varsigma_2}{|\mathbf{r}_1 - \mathbf{r}_2|} \chi_c^*(\varsigma_2) \chi_d(\varsigma_2), \\ \hat{K}_{cd} |e\rangle &\stackrel{\text{def}}{=} \chi_d(\varsigma_1) \int \frac{d\varsigma_2}{|\mathbf{r}_1 - \mathbf{r}_2|} \chi_c^*(\varsigma_2) \chi_e(\varsigma_2) \equiv \hat{J}_{ce} |d\rangle, \end{aligned} \quad (\text{A1})$$

where $\varsigma_{1,2}$ refer to both the spatial and spin coordinates.

2. Scaling the Spin–Orbit Interaction

The explicit form of the RECP (2) is

$$\begin{aligned} \hat{V}^{\text{RECP}}(r) &= \hat{V}^{\text{scalar}}(r) + \mu \hat{V}_{\ell j}^{\text{s-o}}(r), \\ \hat{V}^{\text{scalar}}(r) &\stackrel{\text{def}}{=} -\frac{Q}{r} + \hat{V}_\ell(r) \hat{P}_\ell, \\ \hat{V}_\ell(r) &\stackrel{\text{def}}{=} \frac{1}{2\ell+1} [\ell \hat{V}_{\ell, |\ell-\frac{1}{2}|}(r) + (\ell+1) \hat{V}_{\ell, \ell+\frac{1}{2}}(r)], \\ \hat{P}_\ell &\stackrel{\text{def}}{=} \hat{P}_{\ell, |\ell-\frac{1}{2}|} + \hat{P}_{\ell, \ell+\frac{1}{2}}, \\ \hat{V}_{\ell j}^{\text{s-o}}(r) &\stackrel{\text{def}}{=} \frac{\Delta \hat{V}_\ell(r)}{2\ell+2} [\ell \hat{P}_{\ell, \ell+1/2} - (\ell+1) \hat{P}_{\ell, \ell-1/2}], \\ \Delta \hat{V}_\ell(r) &\stackrel{\text{def}}{=} \hat{V}_{\ell, \ell+1/2}(r) - \hat{V}_{\ell, \ell-1/2}(r), \\ \hat{V}_{\ell j} &\stackrel{\text{def}}{=} B_{\ell j}^k \exp\left(-\beta_{\ell j}^k r^2\right), \end{aligned} \quad (\text{A2})$$

where $Q = 26$ is the residual charge, $\hat{P}_{\ell j}$ is a projector on the spin–angular symmetry ℓj , and $B_{\ell j}^k$ and $\beta_{\ell j}^k$ are numeric coefficients found by fitting to multiconfigurational Dirac–Fock all-electron calculations of the excited spectrum [18, 19].

In Figure 5, we show the effect of scaling the spin–orbit interaction in the RECP (A2). The resultant spin–orbit splitting is essentially proportional to μ . In Table I, the calculated ionization potentials for the case $\mu = 1$ are compared with experimental values from the literature.

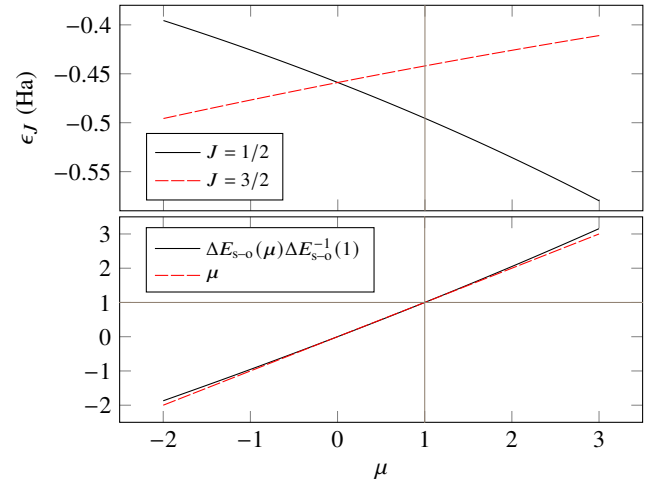


FIG. 5. Spin–orbit splitting $\Delta E_{s-o}(\mu) \stackrel{\text{def}}{=} \epsilon_{3/2}(\mu) - \epsilon_{1/2}(\mu)$ between $5p_{3/2}^{-1}$ and $5p_{1/2}^{-1}$, as a function of the scaling parameter μ in Equation (2).

3. Photoelectron Spectra

The photoelectron distributions, resolved on ion state I , photoelectron energy E , the angle θ with respect to the polarization axis, and with spin projection σ_z , are obtained by

TABLE I. Calculated ionization potentials of the 5s, 5p electrons of xenon, compared with their experimental and RCIS values (Refs: [20]^a, [21]^b, [13]^c).

Hole	I_p (eV)	Exp. (eV)	Δ (eV)	RCIS I_p (eV)
5p _{3/2} ⁻¹	12.026	12.130 ^a	-0.104	11.968 ^c
5p _{1/2} ⁻¹	13.483	13.436 ^b	0.047	13.404 ^c
5s _{1/2} ⁻¹	27.927	23.397 ^b	4.530	27.485 ^c

tracing over the reduced density matrix:

$$P_{I\sigma_z}(E, \theta) \stackrel{\text{def}}{=} \int d\phi \langle \sigma_z | \hat{\rho}_{II}(E, \theta, \phi) | \sigma_z \rangle. \quad (\text{A3})$$

The density matrix is formed from the outer product of the wavefunction with itself,

$$\hat{\rho}(E, \theta, \phi) \stackrel{\text{def}}{=} |\Psi(\mathbf{k})\rangle\langle\Psi(\mathbf{k})|, \quad (\text{A4})$$

using the close-coupling *Ansatz* [22] for the wavefunction

$$|\Psi(\mathbf{k})\rangle = c_{I\mathbf{k}\sigma_z} \mathcal{A} |I\rangle |k\sigma_z\rangle \quad (\text{A5})$$

where $|I\rangle$ is the state of the ion,

$$\mathbf{k} = \begin{bmatrix} k \sin \theta \cos \phi \\ k \sin \theta \sin \phi \\ k \cos \theta \end{bmatrix}, \quad k = \sqrt{2E},$$

is the asymptotic momentum of the photoelectron, σ_z the spin projection of the photoelectron, and \mathcal{A} the antisymmetrization operator. The reduced density matrix is obtained from the full density matrix, by projecting on specific ion states:

$$\hat{\rho}_{IJ} \stackrel{\text{def}}{=} \langle I | \hat{\rho} | J \rangle. \quad (\text{A6})$$

The decomposition (A5) is computed [12] using the tSURFF [23–27] and iSURFV [28] techniques.

Appendix B: Classical Trajectories

Here we re-derive the classical trajectories of a free electron in a monochromatic electric field

$$\mathbf{F}(t) = \mathbf{F}_0 \cos(\omega t);$$

these results have been presented many times, most notably by Corkum [29].

We introduce the free oscillation range and the velocity amplitude:

$$\alpha \stackrel{\text{def}}{=} \frac{F_0}{\omega^2}; \quad v_0 \stackrel{\text{def}}{=} \frac{F_0}{\omega};$$

(we note that $v_0^2 = 4U_p$), as well as the phases $\phi = \omega t$, $\phi_i = \omega t_i$, and $\phi_r = \omega t_r$, $\delta\phi = \phi_r - \phi_i \equiv \omega\tau$, etc.

We find the trajectories by integrating Newton's equations $\mathbf{a}(t) = -\mathbf{F}(t)$, neglecting the influence of the atomic potential:

$$\mathbf{v}(t) = -\mathbf{F}_0 \int_{t_i}^t dt' \cos \phi' = -v_0 (\sin \phi - \sin \phi_i),$$

$$\mathbf{r}(t) = \mathbf{r}_0 + \alpha [\cos \phi - \cos \phi_i + (\phi - \phi_i) \sin \phi_i].$$

The phase of ionization ϕ_i is found for each rescattering phase ϕ_r by requiring that the electron returns to the origin before rescattering:

$$\mathbf{r}(t_r) = 0,$$

which we solve numerically using the gradient method.

The kinetic energy of the electron (before rescattering) is given by

$$W_k(t) = \frac{v^2(t)}{2} \equiv 2U_p (\sin \phi - \sin \phi_i)^2. \quad (\text{B1})$$

TABLE II. Influence of the initial position on the maximal kinetic energy upon rescattering, for $F_0 = 3.5408 \times 10^{-2}$ au and $\omega = 0.0535$ Ha.

Barrier	r_0 (Bohr)	$W_{k,\text{max}}$ (U_p)	ϕ_i (rad)	ϕ_r (rad)	$\delta\phi$ (rad)
None	0.0	3.17	0.31	4.40	4.08
Triangular	-12.96	4.69	0.68	4.27	3.59
Coulomb	-10.49	4.36	0.59	4.30	3.71

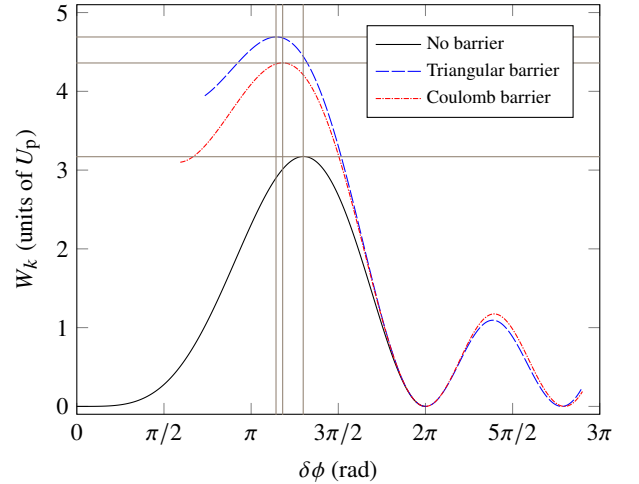


FIG. 6. Kinetic energy upon rescattering as function of excursion phase, for three different choices of initial starting position (given in Table II).

We may choose the initial position at the tunnel exit

$$r_0^{\text{tri}} = -\frac{I_p}{F_0}, \quad \text{or} \quad (\text{B2})$$

$$r_0^{\text{Coul}} = -\frac{I_p}{2F_0} - \sqrt{\left(\frac{I_p}{2F_0}\right)^2 - \frac{2I_p}{F_0}},$$

which will give maximal kinetic energies at the time of rescattering, rather different from when the electron starts at the origin $r_0 = 0$ (see Table II and Figure 6), and in turn influence the final momenta on the detector which upon rescattering had the maximal kinetic energy (see Figure 7). Accounting for the initial position is an important improvement compared to starting at the origin as done by Spanner *et al.* [17], since it allows us to correctly sample the off-axis spin-flip features as seen in Figure 1 of the main text; for the figures shown there, we use the initial position r_0^{Coul} for a Coulombic barrier.

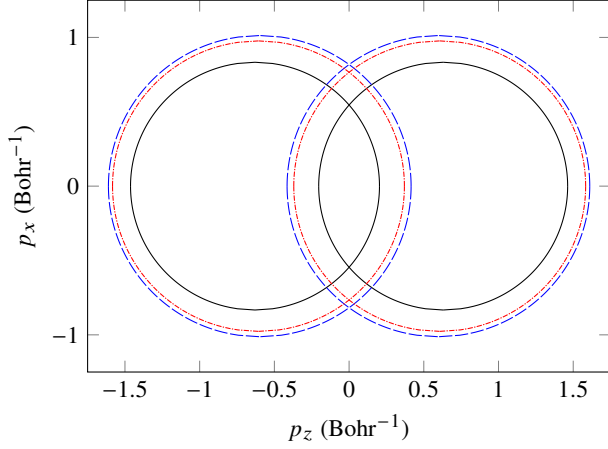


FIG. 7. Final electron momenta corresponding to maximal kinetic energy upon rescattering, for three different choices of initial starting position (line patterns are the same as in Figure 6).

1. Lineouts in the Backward Emission Direction

In Figure 8, the lineouts along the $W_{k,\text{max}}$ circles in the backward emission direction are shown. Due to the long pulse duration ($\tau = 15$ fs), the spin polarization in the backward direction is almost a perfect mirror image of the forward distribution, as evidenced by the similarity of the integrated lineouts also shown in the figure.

Appendix C: Scattering Matrix Elements

1. Effect of Removing \hat{K}_{mm}

See Figure 9 for the effect of removing \hat{K}_{mm} from the EOMs; the results do not change appreciably.

2. Time-Dependent Scattering Matrix Elements

Our numerical treatment is done in the jj coupling basis. We wish to derive an expression for the time-dependent spin flip. The natural basis for this process, the spin-orbit clock, is LS coupling, where the spin of the hole is “breathing” in

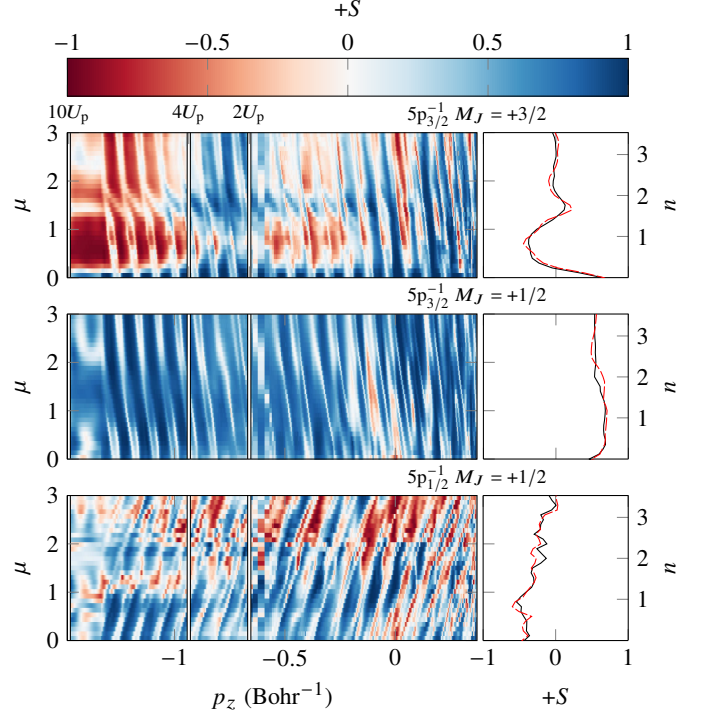


FIG. 8. Similar to Figure 3 of the main manuscript, but the lineouts are instead along the $W_{k,\text{max}}$ circles in the backward direction, i.e. negative final p_z .

time, due to the non-diagonal ionic Hamiltonian. For the np^6 -multiplet, the transform between LS and jj coupling is given by [see Table 8.1 of 30]

j	m_j	$p_{+\alpha}$	$p_{+\beta}$	$p_{0\alpha}$	$p_{0\beta}$	$p_{-\alpha}$	$p_{-\beta}$
$\frac{3}{2}$	$\frac{3}{2}$	1					
$\frac{3}{2}$	$\frac{1}{2}$		$\sqrt{\frac{1}{3}}$	$\sqrt{\frac{2}{3}}$			
$\frac{1}{2}$	$\frac{1}{2}$		$\sqrt{\frac{2}{3}}$	$-\sqrt{\frac{1}{3}}$			
$\frac{3}{2}$	$-\frac{1}{2}$			$\sqrt{\frac{2}{3}}$	$\sqrt{\frac{1}{3}}$		
$\frac{1}{2}$	$-\frac{1}{2}$			$\sqrt{\frac{1}{3}}$	$-\sqrt{\frac{2}{3}}$		
$\frac{3}{2}$	$-\frac{3}{2}$						1

(C1)

which clearly shows that the $J = \frac{3}{2}$, $M_J = \pm\frac{3}{2}$ channels are spin-pure. Similarly, the ionic spin-orbit Hamiltonian within this multiplet is in jj coupling

$$\hat{H}_{s-o}^{(jj)} = \begin{bmatrix} 0 & & & & & & & & \\ & 0 & & & & & & & \\ & & -\Delta E_{s-o} & & & & & & \\ & & & 0 & & & & & \\ & & & & & & & & \\ & & & & & & -\Delta E_{s-o} & & \\ & & & & & & & & 0 \end{bmatrix}, \quad (C2)$$

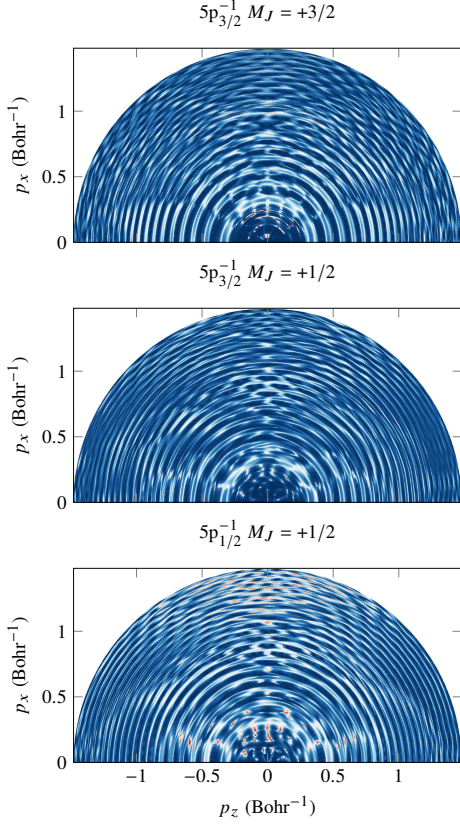


FIG. 9. The effect of removing \hat{K}_{mm} from the EOMs does not appreciably affect the spin-flipping mechanism; cf. Figure 4 of the main manuscript.

the propagator of which in LS coupling is given exactly by

$$\exp\left[-i\hat{H}_{s-o}^{(LS)}(t-t_i)\right] = \begin{bmatrix} 1 & & & & \\ & a & b & & \\ & b & c & & \\ & & & c & b \\ & & & b & a \\ & & & & & 1 \end{bmatrix}, \quad (\text{C3})$$

where

$$a \stackrel{\text{def}}{=} \frac{1}{3}(1 + 2e^{i\phi}), \quad b \stackrel{\text{def}}{=} \frac{\sqrt{2}}{3}(1 - e^{i\phi}), \quad c \stackrel{\text{def}}{=} \frac{1}{3}(2 + e^{i\phi}), \quad (\text{C4})$$

and $\phi = \Delta E_{s-o}(t-t_i)$.

The matrix element responsible for the inelastic scattering between channels is given by

$$[l\tilde{k}|k\tilde{l}] \equiv [l\tilde{k}|k\tilde{l}] - [l\tilde{k}|\tilde{l}k], \quad (\text{C5})$$

the first term of which corresponds to the *direct interaction*, and the second term to the *exchange interaction*. As shown in the above, when dropping \hat{J}_{lk} from the EOMs, the spin-flipping mechanism was almost completely suppressed, which is why we will focus on $[l\tilde{k}|k\tilde{l}]$, from which \hat{J}_{lk} originates [12].

Assume we initially ionize the $|l(t_i)\rangle = |p_+\beta\rangle$ orbital (a component of the $j = 3/2, m_j = 1/2$ orbital); then, neglecting any effect of the spin-orbit interaction on the free electron, $|\tilde{l}\rangle$ will be a β electron, while the associated hole will evolve in time according to

$$|l(t)\rangle = a |p_+\beta\rangle + b |p_0\alpha\rangle. \quad (\text{C6})$$

Simultaneously, the channel we consider scattering *into*, the spin-pure $j = 3/2, m_j = 3/2$, has a time-independent hole, also in LS coupling:

$$|k(t)\rangle = |p_+\alpha\rangle. \quad (\text{C7})$$

From this, we deduce that the direct part of the scattering matrix element (C5), responsible for the apparent spin flip, is

$$\begin{aligned} |[l\tilde{k}|k\tilde{l}]|^2 &= \left| a \underbrace{[p_+\beta; \tilde{k}\sigma_z|p_+\alpha; \tilde{l}\beta]}_0 + b [p_0\alpha; \tilde{k}\sigma_z|p_+\alpha; \tilde{l}\beta] \right|^2 \\ &= \left| \frac{\sqrt{2}}{3}(1 - e^{i\phi}) \right|^2 |[p_0\alpha; \tilde{k}\sigma_z|p_+\alpha; \tilde{l}\beta]|^2 \delta_{\sigma_z\beta} \\ &= \frac{4}{9} [1 - \cos \Delta E_{s-o}(t-t_i)] |[p_0\alpha; \tilde{k}\sigma_z|p_+\alpha; \tilde{l}\beta]|^2 \delta_{\sigma_z\beta}, \end{aligned} \quad (\text{C8})$$

which will have its maximum when $\Delta E_{s-o}(t-t_i) = (2q+1)\pi$, i.e. odd multiples of π .

We would reach a similar conclusion, if we instead assumed ionization to start from $|l(t_i)\rangle = |p_0\beta\rangle$. This argument can trivially be extended to the exchange interaction $[l\tilde{k}|\tilde{l}k]$, and hence also $|[l\tilde{k}|k\tilde{l}]|^2$. As a side-note, since the orbitals in the first coordinate of $[l\tilde{k}|k\tilde{l}]$ in (C8) are both p electrons, only even orders in the multipole expansion of \hat{J}_{lk} will contribute. Furthermore, since the orbitals have different components (p_0 versus p_+), the lowest order is the quadrupole.